*This research has received funding from the European Union under grant agreement No 101099717 – ECOLEFINS project and UK Research and Innovation (UKRI) under the UK governments Horizon Europe funding Guarantee (10079292). Views and opinions expressed are however those of the author(s) only and do not necessarily reflect those of the European Union or European Innovation Council and SMEs Executive Agency (EISMEA) or UK Research and Innovation granting authorities. Neither the European Union nor the granting authorities can be held responsible for them.*

# Deliverable Number: D1.2

# Deliverable Name: Midterm progress on CFD ci-EMR single cell/stack model development

**Dissemination Level: PU – Public**

*Grant Agreement No: 101099717*

*European Innovation Council and SMEs Executive Agency (EISMEA)*
*European Innovation Council (EIC)-E.1 EIC Pathfinder*

ECOLEFINS
CO-IONICS FOR CARBON NEGATIVE PETROCHEMICALS

Funded by the European Union

*This research has received funding from the European Union under grant agreement No 101099717 – ECOLEFINS project and UK Research and Innovation (UKRI) under the UK governments Horizon Europe funding Guarantee (10079292). Views and opinions expressed are however those of the author(s) only and do not necessarily reflect those of the European Union or European Innovation Council and SMEs Executive Agency (EISMEA) or UK Research and Innovation granting authorities. Neither the European Union nor the granting authorities can be held responsible for them.*

# Document Control Sheet

| | |
|---|---|
| ***Project name*** | Nano-Engineered Co-Ionic Ceramic Reactors for $CO_2$/$H_2O$ Electro-conversion to Light Olefins |
| ***Project acronym*** | ECOLEFINS |
| ***Grant Agreement n.*** | 101099717 |
| ***Deliverable No*** | D1.2 |
| ***Deliverable Name*** | Midterm progress on CFD ci-EMR single cell/stack model development |
| ***Lead Beneficiary*** | 4 - POLITO |
| ***Work Package No*** | WP1 |
| ***Type*** | R – Document, Report |
| ***Dissemination Level*** | PU – Public |

| Version | Date | Description |
|---|---|---|
| 2.0 | 29.03.2025 | This deliverable contains the efforts up to M18 associated with the 3D modeling of both planar and tubular ci-EMR cell configurations to co-electrolyze $CO_2$ and $H_2O$ toward light olefins production, by implementing a membrane model to analyze ionic transport, and simulating electrochemical reactions within the electrodes. Additionally, it explores the thermocatalytic production of olefins through MTO (Methanol to Olefins) and FTO (Fischer-Tropsch to Olefins) processes. |

| | |
|---|---|
| ***Date*** | 08.04.2025 |
| ***Number of pages*** | 27 |
| ***Archive name*** | Deliverable D1.2: Midterm progress on CFD ci-EMR single cell/stack model development |
| ***Authors*** | Andrea Moranti, Domenico Ferrero, Massimo Santarelli (POLITO) |
| ***Contributors*** | Andrea Moranti, Domenico Ferrero, Massimo Santarelli (POLITO) |
| ***Reviewer(s)*** | George Marnellos |

ECOLEFINS
CO-IONICS FOR CARBON NEGATIVE PETROCHEMICALS

UK Research and Innovation

Funded by the European Union

*This research has received funding from the European Union under grant agreement No 101099717 – ECOLEFINS project and UK Research and Innovation (UKRI) under the UK governments Horizon Europe funding Guarantee (10079292). Views and opinions expressed are however those of the author(s) only and do not necessarily reflect those of the European Union or European Innovation Council and SMEs Executive Agency (EISMEA) or UK Research and Innovation granting authorities. Neither the European Union nor the granting authorities can be held responsible for them.*

# Document History

| Revision Version | Date | Changes | Changes made by partner |
|---|---|---|---|
| **1.0** | 17/03/2025 | First release | POLITO: first draft |
| **2.0** | 29/03/2025 | Second Version | POLITO: updated template, revised text, added: Tables of Contents, List of Figures, Executive summary, Conclusions |
| **3.0** | 08/04/2025 | Final Version | CERTH: Proofread |
| | | | |
| | | | |
| | | | |

ECOLEFINS
CO-IONICS FOR CARBON NEGATIVE PETROCHEMICALS

UK Research and Innovation

Funded by the European Union

*This research has received funding from the European Union under grant agreement No 101099717 – ECOLEFINS project and UK Research and Innovation (UKRI) under the UK governments Horizon Europe funding Guarantee (10079292). Views and opinions expressed are however those of the author(s) only and do not necessarily reflect those of the European Union or European Innovation Council and SMEs Executive Agency (EISMEA) or UK Research and Innovation granting authorities. Neither the European Union nor the granting authorities can be held responsible for them.*

# Table of Contents

Funded by the European Union

*This research has received funding from the European Union under grant agreement No 101099717 – ECOLEFINS project and UK Research and Innovation (UKRI) under the UK governments Horizon Europe funding Guarantee (10079292). Views and opinions expressed are however those of the author(s) only and do not necessarily reflect those of the European Union or European Innovation Council and SMEs Executive Agency (EISMEA) or UK Research and Innovation granting authorities. Neither the European Union nor the granting authorities can be held responsible for them.*

# List of Figures

UK Research and Innovation
Funded by the European Union

*This research has received funding from the European Union under grant agreement No 101099717 – ECOLEFINS project and UK Research and Innovation (UKRI) under the UK governments Horizon Europe funding Guarantee (10079292). Views and opinions expressed are however those of the author(s) only and do not necessarily reflect those of the European Union or European Innovation Council and SMEs Executive Agency (EISMEA) or UK Research and Innovation granting authorities. Neither the European Union nor the granting authorities can be held responsible for them.*

## Executive Summary

The ECOLEFINS project, supported by the Horizon Europe Innovation Council's EIC Pathfinder program, aims to develop innovative nano-engineered co-ionic ceramic reactors for converting $CO_2$ and $H_2O$ into light olefins. This document details the advancements in modelling and simulating these reactors, utilizing a multi-physics approach that encompasses fluid dynamics, thermal management, electrical behavior, and chemical reactions.

The project involves creating a 3D model for both planar and tubular cell configurations, implementing a membrane model to analyze ionic transport, and simulating electrochemical reactions within the electrodes. Additionally, it explores the thermocatalytic production of olefins through MTO (Methanol to Olefins) and FTO (Fischer-Tropsch to Olefins) processes.

Key findings highlight the impact of different cell configurations on ionic flux distribution, temperature management, and olefin production rates. The study emphasizes on optimizing operating conditions such as temperature, humidification, and flow rates to enhance reactor performance and efficiency.

This research contributes to developing sustainable technologies for olefin production, aligning with broader goals of reducing carbon emissions and promoting a circular economy.

*This research has received funding from the European Union under grant agreement No 101099717 – ECOLEFINS project and UK Research and Innovation (UKRI) under the UK governments Horizon Europe funding Guarantee (10079292). Views and opinions expressed are however those of the author(s) only and do not necessarily reflect those of the European Union or European Innovation Council and SMEs Executive Agency (EISMEA) or UK Research and Innovation granting authorities. Neither the European Union nor the granting authorities can be held responsible for them.*

## Model Overview

For the development of Task 1.2, a multi-physics fluidic, thermal, electric and chemical model for a co-ionic ceramic cell has been implemented and applied to both planar and tubular cell geometry.

At the current stage, the motion of three defects through the membrane has been considered since this kind of material is known to show electronic leakage with related losses in performance. In addition to the proton ions ($H^+$) and the oxygen ones ($O^{2-}$), useful for the production of olefins as defined in the framework of this project, also the electron holes have been considered. This last type of defect, in fact, is considered to typically generate losses in the performance of the yttrium-doped barium perovskite materials, due to a decrease in the transference number, and related faradaic efficiency, during the operation of the cell.

The models implemented are:

- *Planar model*

  A 3D configuration for a 5x5 $cm^2$ planar cell, composed, from the outermost to the innermost layers, of: conductor interconnectors with the required channels for streams flow; porous electrodes subdivided into Gas Diffusion Layer (porous with gas transport purposes) and Gas Diffusion Electrode (where the electrochemical reactions are assumed to occur); proton conductor membrane for ions transport. Steam is injected in the anode side, where water splitting occur and oxygen is produced, while on the cathode side $CO_2$ is the main gas injected with production of olefins. The results for this model are provided since being it the most advanced.

- *Tubular model*

  A 3D configuration for a 20 cm long tubular cell with a tube in shell configuration. The cell is composed, again from the outer to the inlet layer, of: conductor interconnector only with current collection purposes, metallic foam in the internal chamber between interconnector and electrode, electrode where water splitting reaction occur, membrane, electrode for olefins production and internal chamber. The cell is closed at one end by glass-ceramic cap, modeled as an insulating boundary, and by a steel header on the other end for gas outlet and inlet. The double chamber sealed configuration is expected to be useful for economic valorization of by-products as oxygen.

Funded by the European Union

*This research has received funding from the European Union under grant agreement No 101099717 – ECOLEFINS project and UK Research and Innovation (UKRI) under the UK governments Horizon Europe funding Guarantee (10079292). Views and opinions expressed are however those of the author(s) only and do not necessarily reflect those of the European Union or European Innovation Council and SMEs Executive Agency (EISMEA) or UK Research and Innovation granting authorities. Neither the European Union nor the granting authorities can be held responsible for them.*

# 1. Model methods

## 1.1 Membrane model

The current model is focused on the ionic motion in the membrane, with the goal of extending it to the electrodes in transient mode by the end of the project. In the membrane, the three mobile charge-carrying defects, written using the Kröger-Vink notation, are assumed to be protons ($\boldsymbol{OH_o^{\cdot}}$), oxygen vacancies ($\boldsymbol{V_o^{\cdot\cdot}}$) and electron holes ($\boldsymbol{h^{\cdot}}$) [1]. Additionally, these electron holes are assumed to interact with a portion of the dopant yttrium in the zirconium site ( $\boldsymbol{Y'_{Zr}}$), producing a trapped polaron ($\boldsymbol{Y'_{Zr} - O_o^{\cdot}}$). The neutral oxygen site ($O_O^x$) is also considered to ensure charge balance within the perovskite structure.

The model setup and parameter selection for BZY electrolyte materials are based on literature data, particularly from Zhu et al. [2] ensuring consistency with experimentally validated thermodynamic and transport properties. The incorporation reactions occurring at the gas-electrolyte interface are modelled using equilibrium constants ($K_P$), defined in terms of gas partial pressure ($p$). These reactions can be expressed as follows:

- Interface with hydrogen:

$$\frac{1}{2}H_2 + O_o^{\cdot} \leftrightarrow OH_o^{\cdot} \quad (1)$$

$$K_{P,H2} = \frac{[OH_o^{\cdot}]_L}{[O_o^{\cdot}]_L \cdot p_{H2}^{1/2}} \quad (2)$$

- Interface with oxygen:

$$\frac{1}{2}O_2 + O_o^x + V_o^{\cdot\cdot} \leftrightarrow 2O_o^{\cdot} \quad (3)$$

$$K_{P,O2} = \frac{[O_o^{\cdot}]_L^2}{[O_o^x]_L \cdot [V_o^{\cdot\cdot}]_L \cdot p_{O2}^{1/2}} \quad (4)$$

- Interface with water:

$$H_2O + V_o^{\cdot\cdot} + O_o^x \leftrightarrow 2OH_o^{\cdot} \quad (5)$$

$$K_{P,H2O} = \frac{[OH_o^{\cdot}]_L^2}{[O_o^x]_L \cdot [V_o^{\cdot\cdot}]_L \cdot p_{H2O}} \quad (6)$$

- Polaron trapping:

$$Y'_{Zr} + O_o^{\cdot} \leftrightarrow (Y'_{Zr} - O_o^{\cdot}) \quad (7)$$

*This research has received funding from the European Union under grant agreement No 101099717 – ECOLEFINS project and UK Research and Innovation (UKRI) under the UK governments Horizon Europe funding Guarantee (10079292). Views and opinions expressed are however those of the author(s) only and do not necessarily reflect those of the European Union or European Innovation Council and SMEs Executive Agency (EISMEA) or UK Research and Innovation granting authorities. Neither the European Union nor the granting authorities can be held responsible for them.*

$$K_{P,Trap} = \frac{[(Y'_{Zr} - O^{\cdot}_{o})]_L}{[Y'_{Zr}]_L \cdot [O^{\cdot}_{o}]_L} \quad (8)$$

Here, the subscript (L) denotes the formula unit concentration, which can be estimated using:

$$[X_k]_L = [X_k] \cdot V_m \quad (9)$$

where $V_m$ is the lattice molar volume of the perovskite, with a value of $4.57 \cdot 10^{-5}\,\frac{m^3}{mol}$ for the BZY20 considered as preliminary material for this model. The equilibrium constants are evaluated as:

$$K_P = \exp\left(\frac{\Delta S^{\circ}}{R}\right) exp\left(-\frac{\Delta \mathrm{H}^{\circ}}{RT}\right) \quad (10)$$

All constants are interrelated with each other through the gas-phase reaction: $H_2 + \frac{1}{2}O_2 \leftrightarrow H_2O$, following the relation $K^2_{P,H2}K_{P,O2} = K_{P,H2O}K_{P,GAS-PHASE}$. The equilibrium constants of the reaction occurring are:

$$K_{P,H2} = \frac{K_{P,H2O} \cdot K_{P,GAS-PHASE}}{K_{P,O2}} \quad (11)$$

$$\Delta \mathrm{H}^{\circ}_{\mathrm{H2}} = \frac{\Delta \mathrm{H}^{\circ}_{GAS-PHASE} + \Delta \mathrm{H}^{\circ}_{\mathrm{H2O}} - \Delta \mathrm{H}^{\circ}_{\mathrm{O2}}}{2} \quad (12)$$

$$\Delta \mathrm{S}^{\circ}_{\mathrm{H2}} = \frac{\Delta \mathrm{S}^{\circ}_{GAS-PHASE} + \Delta \mathrm{S}^{\circ}_{\mathrm{H2O}} - \Delta \mathrm{S}^{\circ}_{\mathrm{O2}}}{2} \quad (13)$$

To solve the system of Equations (2), (4), (6) and (8), additional conditions have to be verified at the boundary and inside of the membrane such as:

- Yttrium concentration maintained equal to dopant level ($[Y'_{Zr}]^{\circ}_L = 0.2$):

$$[Y'_{Zr}]_L + (Y'_{Zr} - O^{\cdot}_{o}) = [Y'_{Zr}]^{\circ}_L \quad (14)$$

- Conservation of the oxygen sites per formula unit, in a single perovskite lattice, as equal to 3:

$$[V^{\cdot\cdot}_{o}]_L + [OH^{\cdot}_{o}]_L + [O^{\cdot}_{o}]_L + [O^{\mathrm{x}}_{o}]_L + [(Y'_{Zr} - O^{\cdot}_{o})]_L = 3 \quad (15)$$

-

- Electroneutrality condition:

$$2[V^{\cdot\cdot}_{o}]_L + [OH^{\cdot}_{o}]_L + [O^{\cdot}_{o}]_L - [Y'_{Zr}]_L = 3 \quad (16)$$

Once the defect concentrations at the membrane boundary are determined based on gas-phase composition and partial pressures, their transport inside the membrane is described by the Nernst-Planck-Poisson (NPP) equations. Defect conservation follows, in steady state, $\nabla \cdot J_k = 0$, where $\boldsymbol{J_k}$ is the defect flux, described by the

*This research has received funding from the European Union under grant agreement No 101099717 – ECOLEFINS project and UK Research and Innovation (UKRI) under the UK governments Horizon Europe funding Guarantee (10079292). Views and opinions expressed are however those of the author(s) only and do not necessarily reflect those of the European Union or European Innovation Council and SMEs Executive Agency (EISMEA) or UK Research and Innovation granting authorities. Neither the European Union nor the granting authorities can be held responsible for them.*

Nernst-Planck equation:

$$J_k = -D_k\left(\nabla[X_k] + \frac{z_k F}{RT}[X_k]\nabla\varphi_e\right) \quad (17)$$

where $D_k$ [m²/s] is the diffusivity $D_k = D_k^{\circ}\exp(\frac{-E_k}{RT})$ and $\boldsymbol{z_k}$ is the defect charge (1 for protons and polarons, 2 for oxygen vacancies), while $\boldsymbol{\nabla\varphi_e}$ is the electrostatic potential gradient.

This last term can be related to the local charge density ($\rho$ (C/m3)) depending on the relative permittivity ($\varepsilon_r$) through the Gauss Law shown in (18):

$$\nabla\cdot(\varepsilon_r\varepsilon_o\nabla\varphi) = -\rho = -F\sum z_k[X_k] \quad (18)$$

Finally, the overall conductivity of the electrolyte is expressed using the Nernst-Einstein relation:

$$\sigma = \frac{F^2}{RT}\sum_{k=1}^{K} z_k^2[X_k]D_k \quad (19)$$

At the current state, the model uses thermodynamic parameters for the gas-perovskite equilibrium and for the ions diffusivity for a $BaZr_{0.8}Y_{0.2}$ electrolyte material well known in literature and summarized in Table 1 and

***Table 2***.

***Table 1.*** *Thermodynamic parameters for defect reactions with trapping for the electrolyte material*

| **Reaction** | **BZY20** [2] | **BZY20** [2] |
|---|---|---|
| $\frac{1}{2}H_2 + O_o^{\cdot} \leftrightarrow OH_o^{\cdot}$ | -228.36 | -54.80 |
| $\frac{1}{2}O_2 + O_o^x + V_o^{\cdot\cdot} \leftrightarrow 2O_o^{\cdot}$ | 115.31 | -45.89 |
| $H_2O + V_o^{\cdot\cdot} + O_o^x \leftrightarrow 2OH_o^{\cdot}$ | -93.30 | -100 |
| $Y_{Zr}' + O_o^{\cdot} \leftrightarrow (Y_{Zr}' - O_o^{\cdot})$ | -90.30 | -6.71 |

*This research has received funding from the European Union under grant agreement No 101099717 – ECOLEFINS project and UK Research and Innovation (UKRI) under the UK governments Horizon Europe funding Guarantee (10079292). Views and opinions expressed are however those of the author(s) only and do not necessarily reflect those of the European Union or European Innovation Council and SMEs Executive Agency (EISMEA) or UK Research and Innovation granting authorities. Neither the European Union nor the granting authorities can be held responsible for them.*

***Table 2.*** *Diffusion coefficients of the defects with trapping for the electrolyte material*

| **Defects** | $D_k^{\circ}\left[\frac{m^2}{s}\right]$ | $E_k^{\circ}\left[\frac{kJ}{mol}\right]$ |
|---|---|---|
| | **BZY20** [2] | **BZY20** [2] |
| $OH_o^{\cdot}$ | $5.18 \cdot 10^{-7}$ | 60.66 |
| $V_o^{\cdot\cdot}$ | $2.03 \cdot 10^{-7}$ | 85.19 |
| $O_o^{\cdot}$ | $1.38 \cdot 10^{-5}$ | 7.18 |

These values will be adapted in order to properly represent the electrolyte selected in the project framework. To do this DFT and experimental results from partners, such as Forschungszentrum Jülich, will be used to extrapolate the required parameters.

### 1.2 Gas ducts and interconnects

The model assumes fluid flow occurs in open regions, defining velocity components in two dimensions (u, v) [m/s] and pressure (p) [Pa]. The governing equations include Navier-Stokes for momentum conservation in Newtonian fluids and continuity equations for mass conservation.

Fluid properties, such as density and viscosity, are treated as functions of temperature, composition, and pressure, with the Peng-Robinson equation of state used to describe gas-phase behaviour. The flow within the channels is considered compressible, with reference conditions set at atmospheric pressure and temperature. A no-slip condition is applied at the interconnector walls, while the interface with the membrane is treated separately in the electrode model.

In addition to momentum and mass conservation, Maxwell-Stefan diffusion is implemented to model gas-phase transport within the channels, while species flux is determined using Fick's law. The thermal model accounts for heat generation, transfer, and dissipation during operation, ensuring accurate temperature distribution predictions. For the interconnectors, electrical conduction is modelled using Ohm's law, assuming an equipotential condition with negligible internal resistance.

*This research has received funding from the European Union under grant agreement No 101099717 – ECOLEFINS project and UK Research and Innovation (UKRI) under the UK governments Horizon Europe funding Guarantee (10079292). Views and opinions expressed are however those of the author(s) only and do not necessarily reflect those of the European Union or European Innovation Council and SMEs Executive Agency (EISMEA) or UK Research and Innovation granting authorities. Neither the European Union nor the granting authorities can be held responsible for them.*

The thermal model considers energy balance and simplified heat transfer equation:

$$\rho\, C_p \mathrm{u} \cdot \nabla \mathrm{T} + \nabla \cdot q = Q \qquad (20)$$

With $q$ [W/m$^2$] heat flux and Q [W/m$^3$] additional heat sources. The fluid's thermal conductivity, density, heat capacity, and the ratio of specific heats, as previously introduced, are defined considering a real fluid according to the Peng-Robinson model.

### *1.3* Electrodes

The electrodes are treated as porous media, allowing for the simultaneous transport of electricity, fluids, and reactant gases, as well as enabling electrochemical reactions at the active sites near the membrane. The gas diffusion layer (GDL) facilitates electrical conduction and gas transport, while the gas diffusion electrode (GDE) additionally accounts for the volumetric current density associated with the electrochemical reaction.

Charge conservation is described using Ohm's law, ensuring continuity of current flow across the porous medium. In the GDL, only electronic conduction occurs, while in the GDE, both electronic and ionic conduction are considered. The effective conductivity of the electrolyte phase within the electrodes is lower than in the dense membrane and is scaled by a correction factor (0.4) based on the volume fraction of the active phase. The governing equations for charge transport in the electrodes include:

$$i = -\sigma_{s,eff} \nabla \Phi_{\mathrm{e}} \qquad (21)$$

$$\nabla \cdot \mathrm{i_s} = -i_{v,tot} \qquad (22)$$

Within this equations $\sigma_{s,eff}$ represents the effective electronic conductivity, assumed to be 10000 S/m, while $i_{v,tot}$ (A/m$^3$) indicates the overall volumetric current density due to the electrode reactions and is assumed as null in the GDL.

At the current state Electrode reactions involve both oxidation and reduction processes, with the equilibrium voltage defined based on the Gibbs free energy of reaction and the partial pressures of reactants and products. The equilibrium potential for electrolysis is given by:

$$E_{eq} = \frac{\Delta g_{reac}(t,p_i)}{zF} = -\frac{\Delta g_{reac}(t,p_0)}{zF} - \frac{\mathrm{RT}}{zF} ln \frac{\prod_R (pi/p_{0)}^{v_i}}{\prod_P (pi/p_{0)}^{v_i}} \qquad (23)$$

The activation overvoltage is introduced as $\eta = E_{ct} - E_{eq}$ with $E_{ct} = \Phi_s - \Phi_l$which corresponds to the difference between the electrode and electrolyte electrostatic potential. This overvoltage governs the charge transfer at both electrodes and determines reaction kinetics. The Butler-Volmer equation describes the local current density as:

*This research has received funding from the European Union under grant agreement No 101099717 – ECOLEFINS project and UK Research and Innovation (UKRI) under the UK governments Horizon Europe funding Guarantee (10079292). Views and opinions expressed are however those of the author(s) only and do not necessarily reflect those of the European Union or European Innovation Council and SMEs Executive Agency (EISMEA) or UK Research and Innovation granting authorities. Neither the European Union nor the granting authorities can be held responsible for them.*

$$i_{loc} = i_0 \left( \exp\left(\frac{\alpha_a F \eta}{RT}\right) - exp\left(\frac{-\alpha_c F \eta}{RT}\right)\right) \quad (24)$$

with $i_0$ the exchange current density, $\alpha_a$ and $\alpha_c$ respectively anodic and cathodic transfer coefficient.
The electrode reaction source and the local current are finally linked to one another through the active specific surface area considered to be equal to $10^9$ 1/m.

Gas transport within the porous electrodes follows Fickian diffusion, with porosity-dependent corrections applied using the Bruggeman relation. The governing momentum equation, incorporating inertial effects, is based on the Stokes-Brinkman formulation for porous media. Additionally, heat generation due to irreversibilities is accounted for, representing deviations from the ideal electrochemical reaction and providing insight into thermal management strategies within the electrode structure.

### 1.4 Olefins thermocatalytic production

The current model includes the reaction occurring for the synthesis of the olefins within the cell itself in the porous layer of the cathode. In particular, several reactions, related to the MTO and FTO process are introduced within the GDE. The reactions are listed below, together with their reaction rates, which are calculated using empirical equations and parameters, provided by different sources. In particular, for the reactions of the MTO process using SAPO-34 catalyst, the reference is the paper of Rostami et al [3], for the FTO using FeK-γAlO₂, Najari et al [4], and for the methanol synthesis Leonzio et al, Cu/AlO₃ [5].

***Table 3.*** *Reactions in the MTO process in the cell*

| **MTO (reactions)** [3] | **Reaction rate** |
|---|---|
| $CO_2 + 3H_2 \leftrightarrow CH_3OH + H_2O$ | $\frac{K_1 p_{CO2} p_{H2} (1 - \frac{1}{K_{eq1}} \frac{p_{H2O} p_{CH3OH}}{p_{H2}^3 p_{CO2}}}{\left(1 + K_2 \frac{p_{H2O}}{p_{H2}} + K_3 p_{H2}^{0.5} + K_4 p_{H2O}\right)^3}$ |
| $2\ CH_3OH \leftrightarrow CH_3OCH_3 + H_2O$ | $k_1 \phi_1 p_{CH3OH}^2 - \left(\frac{k_1}{kE}\right) p_{CH3OCH3} p_{H2O}$ |
| $2\ CH_3OCH_3 \rightarrow C_2H_4 + 2\ CH_3OH$ | $k_2 \phi_2 p_{CH3OCH3}^2$ |
| $2\ CH_3OH \rightarrow C_2H_4 + 2\ H_2O$ | $k_3 \phi_3 p_{CH3OH}^2$ |
| $C_2H_4 + CH_3OCH_3 \rightarrow C_3H_6 + CH_3OH$ | $k_4 \phi_4 p_{C2H4} p_{CH3OCH3}$ |
| $C_3H_6 + CH_3OCH_3 \rightarrow C_4H_8 + CH_3OH$ | $k_5 \phi_5 p_{C3H6} p_{CH3OCH3}$ |
| $CH_3OH \rightarrow CO + 2\ H_2$ | $k_7 \phi_7 p_{CH3OH}$ |

Funded by the European Union

*This research has received funding from the European Union under grant agreement No 101099717 – ECOLEFINS project and UK Research and Innovation (UKRI) under the UK governments Horizon Europe funding Guarantee (10079292). Views and opinions expressed are however those of the author(s) only and do not necessarily reflect those of the European Union or European Innovation Council and SMEs Executive Agency (EISMEA) or UK Research and Innovation granting authorities. Neither the European Union nor the granting authorities can be held responsible for them.*

| | |
|---|---|
| $CH_3OH + H_2 \rightarrow CH_4 + H_2O$ | $k_8\phi_8 p_{CH3OH} p_{H2}$ |
| $C_2H_4 + H_2 \rightarrow C_2H_6$ | $k_{10}\phi_{10} p_{C2H4} p_{H2}$ |
| $C_3H_6 + H_2 \rightarrow C_3H_8$ | $k_{11}\phi_{11} p_{C3H6} p_{H2}$ |

***Table 4.*** *Reactions in the FTO process in the cell*

| **FTO + Reverse water gas shift reaction(RWGS)** [4] | **Reaction rate** |
|---|---|
| $CO + 3\,H_2 \rightarrow CH_4 + H_2O$ | $k_{FT,CH4}\frac{p_{CO}p_{H2}}{p_{CO} + a_{sH,H2O}p_{H2O} + b_{sH,CO2}p_{CO2}}$ |
| $2\,CO + 4\,H_2 \rightarrow C_2H_4 + 2\,H_2O$ | $k_{FT,C2H4}\frac{p_{CO}p_{H2}}{p_{CO} + a_{FT,C2H4,H2O}p_{H2O} + b_{FT,CH4,CO2}p_{CO2}}$ |
| $2\,CO + 4\,H_2 \rightarrow C_2H_6 + 2\,H_2O$ | $k_{FT,C2H6}\frac{p_{CO}p_{H2}}{p_{CO} + a_{FT,C2H4,H2O}p_{H2O} + b_{FT,C2H6,CO2}p_{CO2}}$ |
| $3\,CO + 6\,H_2 \rightarrow C_3H_6 + 3\,H_2O$ | $k_{FT,C3H6}\frac{p_{CO}p_{H2}}{p_{CO} + a_{FT,C3H6,H2O}p_{H2O} + b_{FT,C3H6,CO2}p_{CO2}}$ |
| $3\,CO + 7\,H_2 \rightarrow C_3H_8 + 3\,H_2O$ | $k_{FT,C3H8}\frac{p_{CO}p_{H2}}{p_{CO} + a_{FT,C3H8,H2O}p_{H2O} + b_{FT,C3H8,CO2}\,p_{CO2}}$ |
| $4CO + 8\,H_2 \rightarrow C_4H_8 + 4\,H_2O$ | $k_{FT,C4H8}\frac{p_{CO}p_{H2}}{p_{CO} + a_{FT,C4H8,H2O}p_{H2O} + b_{FT,C4H8,CO2}p_{CO2}}$ |
| $CO_2 + H_2 \rightarrow CO + H_2O$ | $k_{sH}\frac{p_{CO2}p_{H2} - p_{CO}p_{H2O}/K_{eq}}{p_{CO} + a_{sh,H2O}p_{H2O} + b_{sH,CO2}p_{CO2}}$ |

Endothermicity and exothermicity of each reaction have also been considered to assess the temperature change in the single repeating unit.

## 2. Future steps

The model set-up is almost complete in terms of governing equations, the future steps will be mainly focused on three key aspects:

- Transient modelling in the electrodes considering ions consumption due electrochemical production and gas-perovskite interaction.
- Calibration of several model parameters (Butler-Volmer pre-exponential, gas-perovskite thermodynamic, ionic diffusivities, olefins thermocatalytic rates) according to data from project's

*This research has received funding from the European Union under grant agreement No 101099717 – ECOLEFINS project and UK Research and Innovation (UKRI) under the UK governments Horizon Europe funding Guarantee (10079292). Views and opinions expressed are however those of the author(s) only and do not necessarily reflect those of the European Union or European Innovation Council and SMEs Executive Agency (EISMEA) or UK Research and Innovation granting authorities. Neither the European Union nor the granting authorities can be held responsible for them.*

partners.

- Accountability for co-ionic behavior also for electrochemical synthesis of olefins.

## 3. Results

The results presented here show CFD model outcomes of planar/tubular ci-EMRs also with the goal of providing useful aid for the optimal operation, and in the future also optimal geometry design.

The main results shown are:

- Cell polarization curve
- Temperature distribution over the planar SRU (assuming only electrochemical hydrogen production)
- Temperature distribution over the tubular SRU considering
- Distribution of the ionic fluxes over the membrane surface with main focus on protons and oxygen ions
- Olefins production from FTO and MTO routes.

Regarding the planar cell, three different configurations have been modeled and are shown. Two configurations consider the flows of gas, in anode and cathode, to be in parallel configurations, respectively co- and counter-flow. A third configuration, instead, considers the cross flow of the streams. The cell is fed by 80%$N_2$+ 20%$H_2$ at the cathode side and 20%$H_2O$+Air at the anode side and is operated at atmospheric pressure.

Planar SRU

Despite three configurations for the planar cells being modeled, only one polarization curve is shown in baseline condition with the flow compositions just introduced, since similar results are obtained with no relevant differences. The main distinction is present between the parallel and cross flow configurations, with a difference, at 1.35V, of 0.03 A/cm$^2$. Almost identical values are instead obtained between the co and counter flows configurations.

*This research has received funding from the European Union under grant agreement No 101099717 – ECOLEFINS project and UK Research and Innovation (UKRI) under the UK governments Horizon Europe funding Guarantee (10079292). Views and opinions expressed are however those of the author(s) only and do not necessarily reflect those of the European Union or European Innovation Council and SMEs Executive Agency (EISMEA) or UK Research and Innovation granting authorities. Neither the European Union nor the granting authorities can be held responsible for them.*

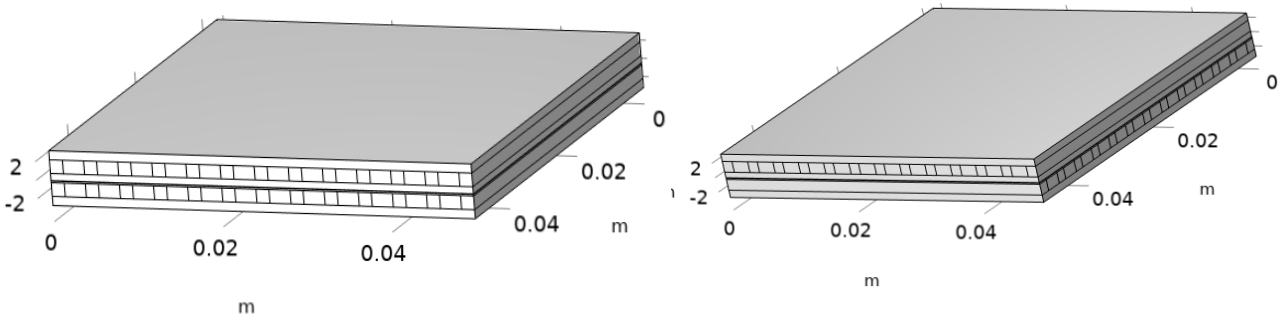


***Figure 1.*** *Geometry for planar SRU in co and counter flow (left) and cross-flow (right)*

### 3.1 Ionic fluxes distribution

In this section the ionic distribution of the two ions on interest, protons ($H^+$) and oxygen ($O^{2-}$), over the electrolyte volume are shown. The two indicators of interest are respectively the homogeneity, the average value and the difference between the two fluxes along the surface. The best outcomes in terms of olefins production are expected to be reached where the highest ionic fluxes are achieved and with a similar distribution, as having the maximum for protons and for oxygen ions in the same positions allow to maintain the ratio of 1:1 optimal for olefins synthesis. Taking into account this two indicators, the cross-flow (Figure 2) and the counter-flow (Figure 4) configurations have the best performance, since the highest fluxes are achieved as highlighted by a direct comparison with the co-flow configuration (Figure 3). Additionally, when taking into account also the ionic flux homogeneity, the cross-flow seems to have also a slightly better performance due to less variable distribution and also due to similar trends between protons and oxygen ions fluxes.

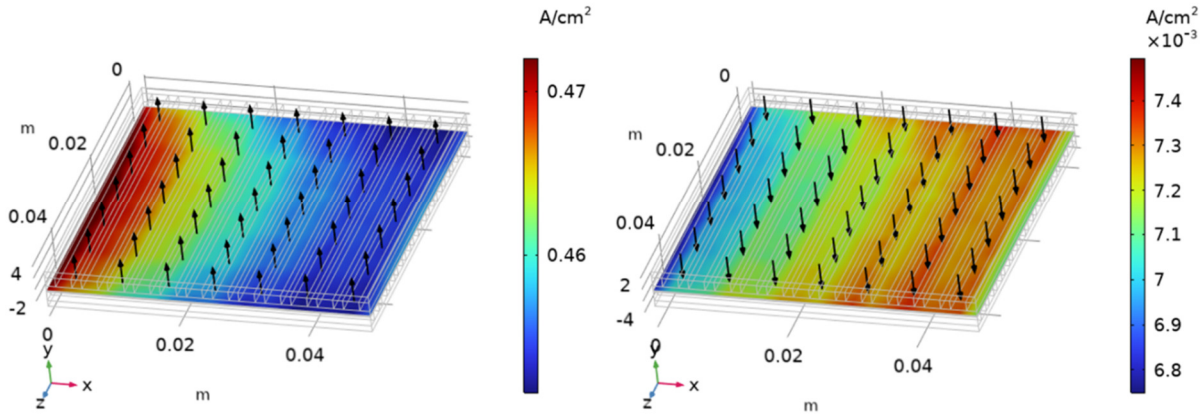


***Figure 2.*** *Protons (left) and oxygen vacancies (right) current densities in cross flow configuration*

*This research has received funding from the European Union under grant agreement No 101099717 – ECOLEFINS project and UK Research and Innovation (UKRI) under the UK governments Horizon Europe funding Guarantee (10079292). Views and opinions expressed are however those of the author(s) only and do not necessarily reflect those of the European Union or European Innovation Council and SMEs Executive Agency (EISMEA) or UK Research and Innovation granting authorities. Neither the European Union nor the granting authorities can be held responsible for them.*

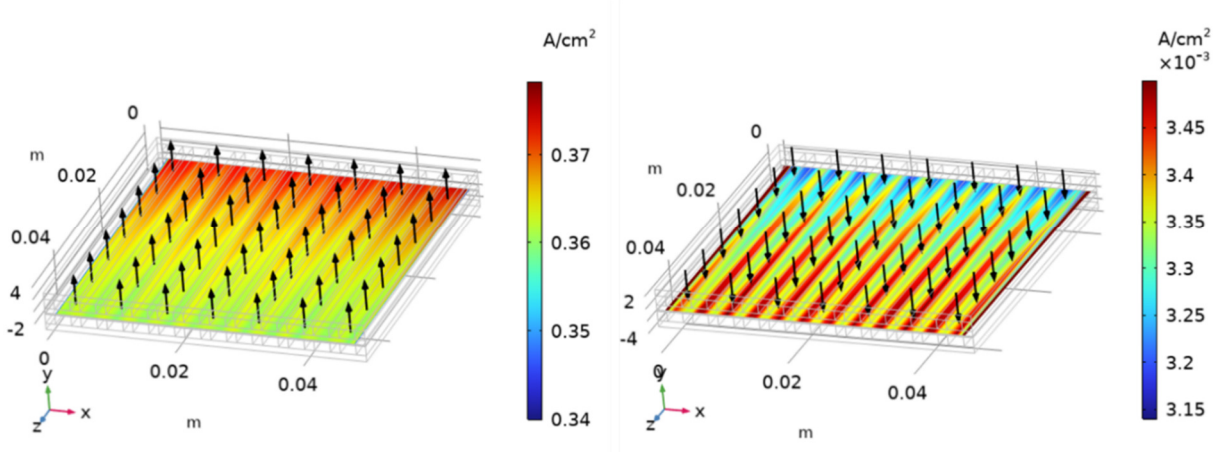


***Figure 3.*** *Protons (left) and oxygen vacancies (right) current densities in co-flow configuration*

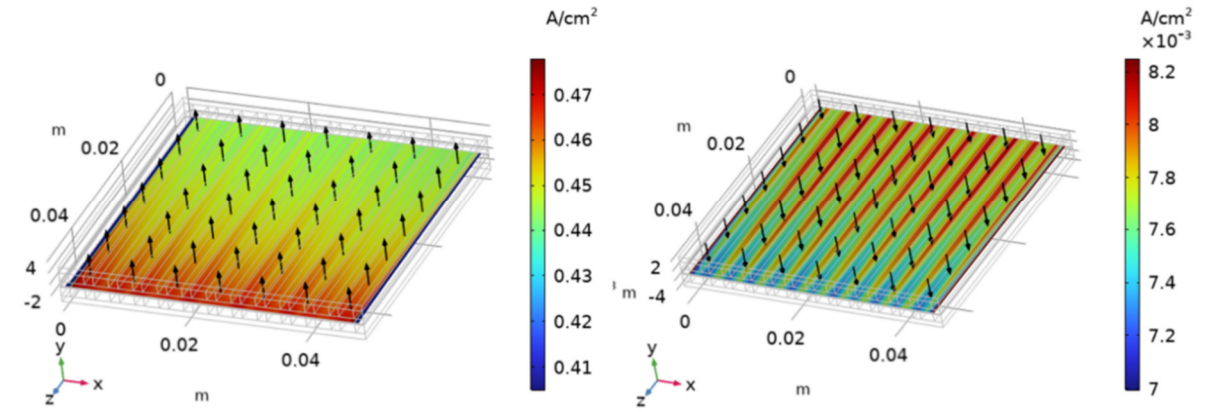


***Figure 4.*** *Protons (left) and oxygen vacancies (right) current densities in counter flow configuration*

Despite this initial trials and results provide useful inputs and aids towards the best configuration and design for the SRU, it is important account for the low oxygen ions fluxes which derives from the assumed electrolyte material (BZY20) for the simulation, which is characterized by a preferable protonic flux, differently from the material being developed in the ECOLEFINS framework. The electrolyte material will be updated when the final cell compositions will be defined in the project.

### 3.2 Temperature distribution

The third result shows the temperature distribution. If the first two indicators shown, represented by the overall and partial current, are mainly associated to the electrochemical performance of the cell, this third indicator is principally linked to what will be the structural behavior and especially to the thermal gradients, and related stresses, that may derive from different thermal expansion of each element composing the SRU. The cross-flow configuration, for example, shows slightly better results, with slightly lower maximum temperatures and lower average temperature over the whole cell. It should be noted that the inlet flow rates are high and allow for a

*This research has received funding from the European Union under grant agreement No 101099717 – ECOLEFINS project and UK Research and Innovation (UKRI) under the UK governments Horizon Europe funding Guarantee (10079292). Views and opinions expressed are however those of the author(s) only and do not necessarily reflect those of the European Union or European Innovation Council and SMEs Executive Agency (EISMEA) or UK Research and Innovation granting authorities. Neither the European Union nor the granting authorities can be held responsible for them.*

good cooling effect on the cell. Lower fluid velocity are expected to increase this differences.

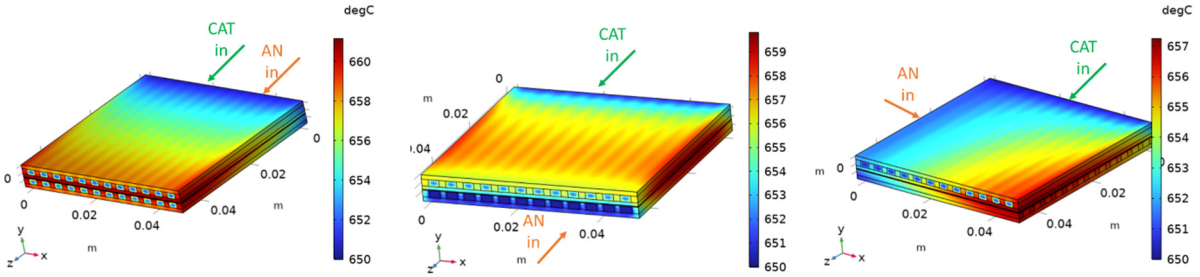


***Figure 5.*** *Temperature distribution in the SRU in co-flow (left), counter-flow (center) and cross-flow (right) configurations*

### 3.3 Olefins production from FTO and MTO routes

In Figure 6 the change in molar fraction of the flowing streams, due to the production of olefins from FTO and MTO routes, over the length of the cell are shown. As already mentioned, the size of the cell was changed with respect to the base case scenario and also between the two routes in order to validate with higher precision the models with the available literature data. It should be noted, in fact, that the kinetic expressions available have been evaluated for fluidized bed which strongly differ from the concept of electrochemical cell also and especially due to the residence time of the fluids in contact with the catalysts. Still, considering the different catalysts, some interesting conclusions and aids for future development have been provided. From the presented images the MTO route seems to be better than the FTO since higher olefins molar fraction at the outlet of the cell is produced. Still it should be noted that in first configuration where FTO is considered, the initial reactant is $CO_2$ which first has to be converted in CO through RWGS which will generate olefins production than MTO where direct methanol injection is assumed. A fitting with available data from other project partner will allow to better interpret this model.

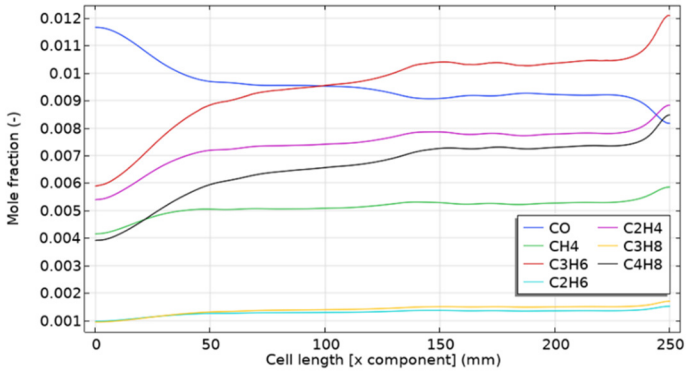

*This research has received funding from the European Union under grant agreement No 101099717 – ECOLEFINS project and UK Research and Innovation (UKRI) under the UK governments Horizon Europe funding Guarantee (10079292). Views and opinions expressed are however those of the author(s) only and do not necessarily reflect those of the European Union or European Innovation Council and SMEs Executive Agency (EISMEA) or UK Research and Innovation granting authorities. Neither the European Union nor the granting authorities can be held responsible for them.*

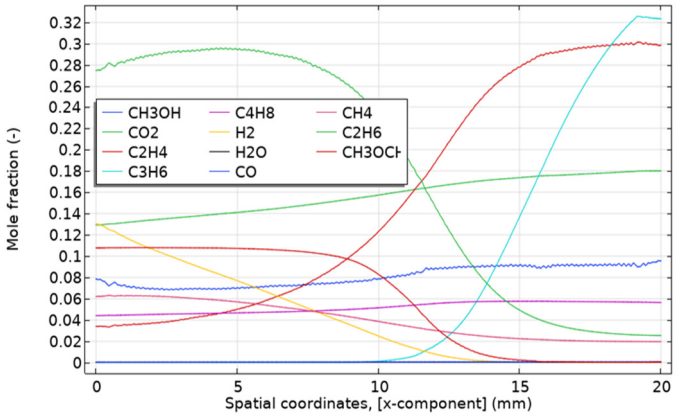


***Figure 6.*** *Hydrocarbons production along cell length from Fischer-Tropsch to Olefins (top) and Methanol to Olefins (bottom) reactions*

## 3.4 Effect of operating conditions on performance

### 3.4.1 Temperature Sensitivity

Operating temperature significantly impacts electrolysis performance, influencing area-specific resistance (ASR), charge carrier mobility, and ionic transport mechanisms. Higher temperatures reduce ASR and enhance overall conductivity, improving efficiency. However, proton and electron hole conductivities respond differently, with electron holes showing greater temperature sensitivity, especially at higher voltage gradients due to their higher diffusivity according to the Nernst-Planck equation to describe the flux of each ion. The proton transference number declines at elevated voltages, with its maximum shifting toward lower voltages as temperature increases, driven by changes in migration contributions. Additionally, higher temperatures reduce membrane hydration, leading to lower proton concentrations and affecting both diffusion and migration mechanisms.

Thermal modelling highlights that internal temperatures can exceed the setpoint by up to 45°C, particularly in regions of higher current density. The counter-flow configuration of reactants influences temperature distribution, with cooling effects from the cathode-side stream helping regulate heat buildup. While modifications in flow rate and inlet temperatures could impact thermal balance, these aspects are not further explored.

### 3.4.2 Cathode Humidification Sensitivity

Increasing water content at the cathode inlet reduces current density at a given voltage, primarily due to changes in hydrogen partial pressure and equilibrium voltage. The corresponding increase in voltage gradient

*This research has received funding from the European Union under grant agreement No 101099717 – ECOLEFINS project and UK Research and Innovation (UKRI) under the UK governments Horizon Europe funding Guarantee (10079292). Views and opinions expressed are however those of the author(s) only and do not necessarily reflect those of the European Union or European Innovation Council and SMEs Executive Agency (EISMEA) or UK Research and Innovation granting authorities. Neither the European Union nor the granting authorities can be held responsible for them.*

across the membrane enhances migration-driven transport, partially counteracting the reduction in diffusion flux. Membrane hydration leads to a higher proton concentration, but electron hole and proton fluxes exhibit distinct responses to water content variations, as reflected in transference number trends. Overall, cathode humidification has a moderate impact on electrolysis performance, with limited influence on charge transport mechanisms compared to anode humidification.

### 3.4.3 Anode Humidification Sensitivity

Anode humidification has a more pronounced effect on performance, as increasing water content enhances equilibrium voltage and reduces polarization losses. The resulting increase in proton concentration at the anode improves protonic current density, while electron hole concentration decreases, minimizing parasitic electronic leakage. This shift optimizes charge transport efficiency, benefiting both diffusion and migration mechanisms. Additionally, higher anode humidification increases the transference number, shifting its peak to lower voltages due to modifications in defect diffusivity and mobility.

Despite the benefits of higher water content, long-term durability must be considered, particularly for ceria-containing electrolytes, which degrade under high-humidity conditions. Optimizing humidification is therefore essential to maximize performance while ensuring material stability over extended operational periods.

### 3.4.4 Oxygen vacancies diffusivity sensitivity

In this section, the ionic diffusivity of the oxygen vacancies, with respect to the hydrogen ions one, is doubled by acting on the pre-exponential term while maintaining the same activation energy in the Arrhenius form to maintain its characteristic dependence on temperature.

The results are extrapolated imposing a voltage of 1.35 V and studying the behaviour for temperatures from 450°C to 650°C with steps of 50°C with cathode stream of 80% N2 + 20% H2 and anode one of 30% H2O+Air.

From Figure 7, the variation in the transference number for OH and Vo depending on the oxygen vacancies diffusivities can be observed. The trend with respect to the temperature show how higher temperature favour the oxygen conduction with respect to the hydrogen one. Furthermore, even though it is not here highlighted, the decrease of the OH transference number at higher temperatures is associated with the electron holes higher mobility at higher temperatures, with corresponding higher electronic leakage.

*This research has received funding from the European Union under grant agreement No 101099717 – ECOLEFINS project and UK Research and Innovation (UKRI) under the UK governments Horizon Europe funding Guarantee (10079292). Views and opinions expressed are however those of the author(s) only and do not necessarily reflect those of the European Union or European Innovation Council and SMEs Executive Agency (EISMEA) or UK Research and Innovation granting authorities. Neither the European Union nor the granting authorities can be held responsible for them.*

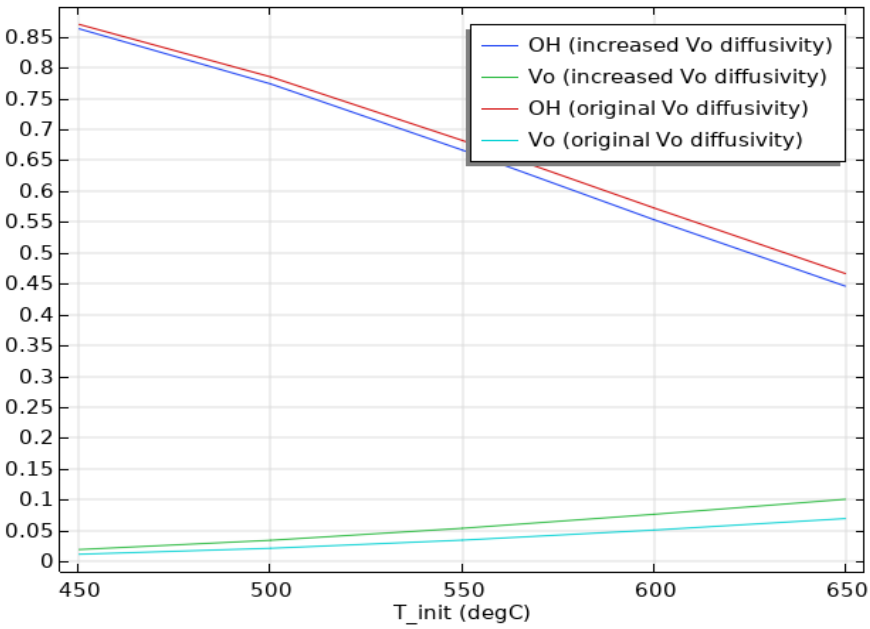


***Figure 7.*** *Transference number depending on oxygen vacancies diffusivity*

Despite the visible increase in oxygen vacancies transference number when higher diffusivities are used, the increase is not huge. In fact, it has been tested and demonstrated how, after a specific threshold of around 1.4 times the original value, the transference number remains constant even when higher values are used.

A plausible explanation is associated to the oxygen vacancies concentration at the electrolyte interface highlighting the importance of selecting a proper electrolyte material also studying on interaction between gas and perovskite for increased oxygen ions formation.

Tubular SRU

From the tubular SRU a focus on the olefins production, and also on thermal management has been made.

*This research has received funding from the European Union under grant agreement No 101099717 – ECOLEFINS project and UK Research and Innovation (UKRI) under the UK governments Horizon Europe funding Guarantee (10079292). Views and opinions expressed are however those of the author(s) only and do not necessarily reflect those of the European Union or European Innovation Council and SMEs Executive Agency (EISMEA) or UK Research and Innovation granting authorities. Neither the European Union nor the granting authorities can be held responsible for them.*

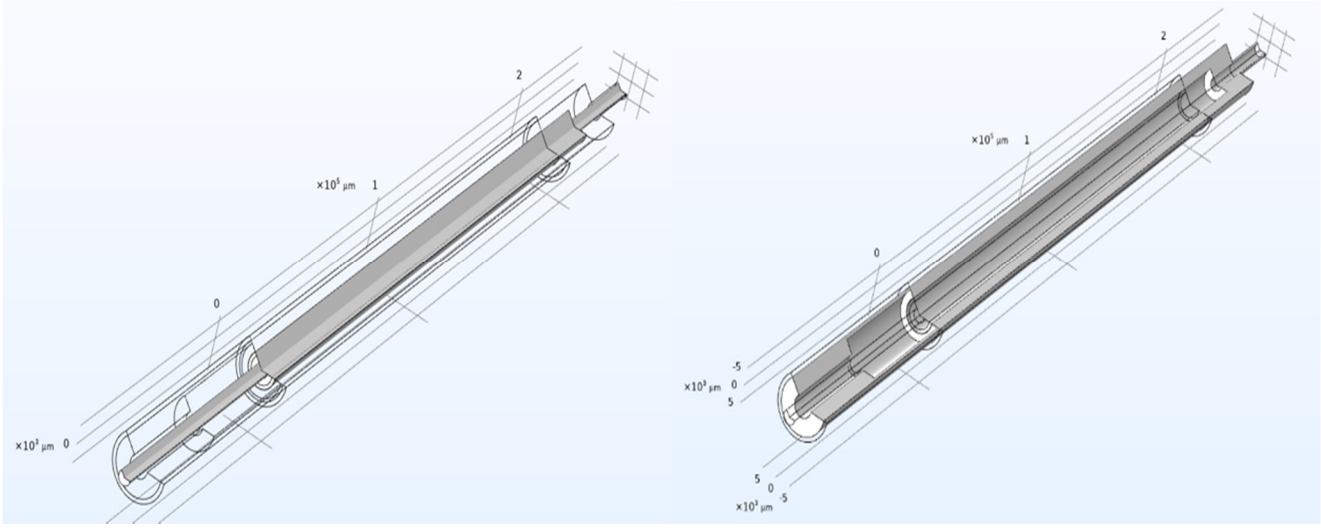

***Figure 8.*** *Geometry for tubular SRU*

### 3.5 Ethylene Production Analysis

An objective of this research is the production of ethylene, which is investigated through simulations at different temperatures under isothermal conditions. These simulations were conducted at 450°C, 500°C, and 550°C. The results indicate that ethylene production decreases with increasing temperature, with outlet ethylene molar fractions of 11.8% at 450°C and 10.5% at 550°C. This trend is attributed to the exothermic nature of both the methanol-to-olefins (MTO) and Fischer Tropsch-to-olefins (FTO) processes, which are favoured at lower temperatures. Typically, the MTO process, known for its higher productivity and selectivity for light olefins, operates optimally between 350-400°C.

However, the electrochemical production of hydrogen via proton-ceramic cells typically occurs at higher temperatures, presenting a limitation for optimal olefin synthesis within the cell.

ECOLEFINS
CO-IONICS FOR CARBON NEGATIVE PETROCHEMICALS
UK Research and Innovation
Funded by the European Union

*This research has received funding from the European Union under grant agreement No 101099717 – ECOLEFINS project and UK Research and Innovation (UKRI) under the UK governments Horizon Europe funding Guarantee (10079292). Views and opinions expressed are however those of the author(s) only and do not necessarily reflect those of the European Union or European Innovation Council and SMEs Executive Agency (EISMEA) or UK Research and Innovation granting authorities. Neither the European Union nor the granting authorities can be held responsible for them.*

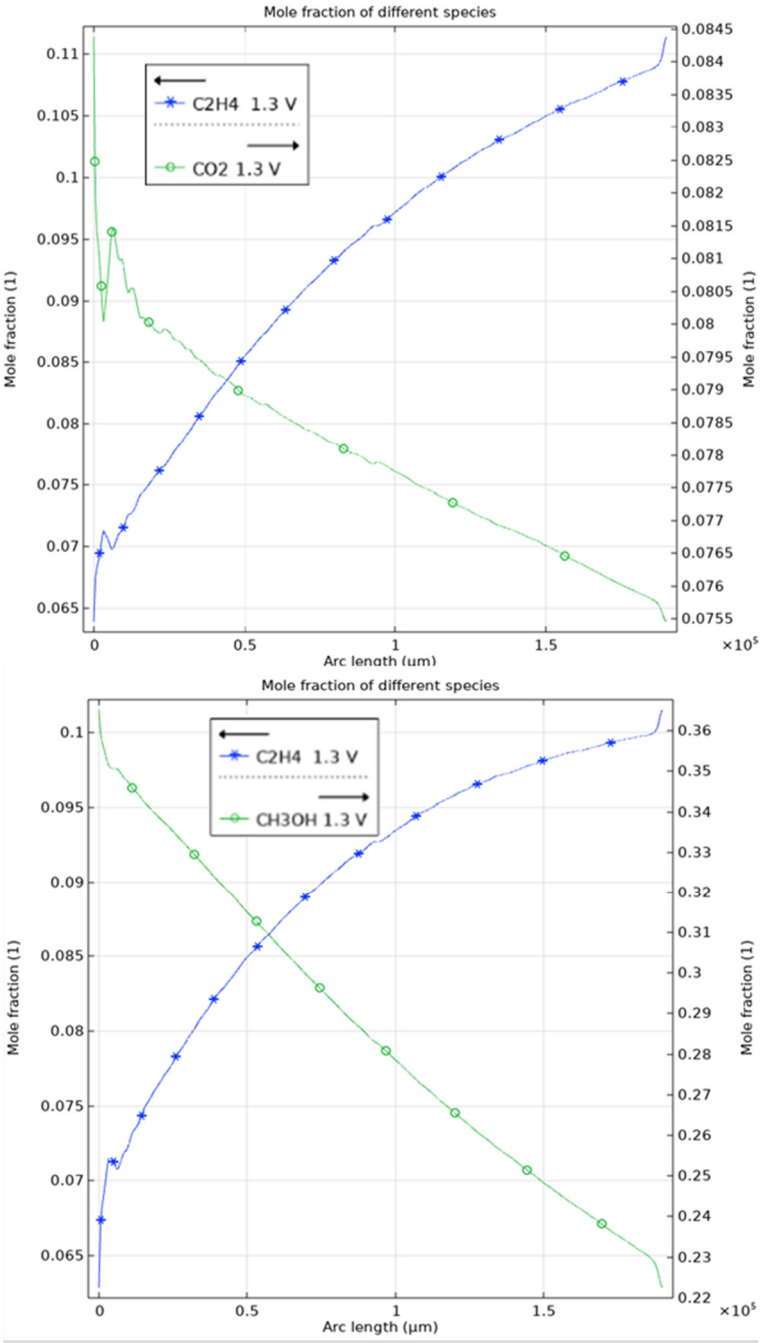


***Figure 9.*** *Mole fraction trend along the axial direction of ethene/$CO_2$ (above) and ethene/methanol (below) at 450°C*

*This research has received funding from the European Union under grant agreement No 101099717 – ECOLEFINS project and UK Research and Innovation (UKRI) under the UK governments Horizon Europe funding Guarantee (10079292). Views and opinions expressed are however those of the author(s) only and do not necessarily reflect those of the European Union or European Innovation Council and SMEs Executive Agency (EISMEA) or UK Research and Innovation granting authorities. Neither the European Union nor the granting authorities can be held responsible for them.*

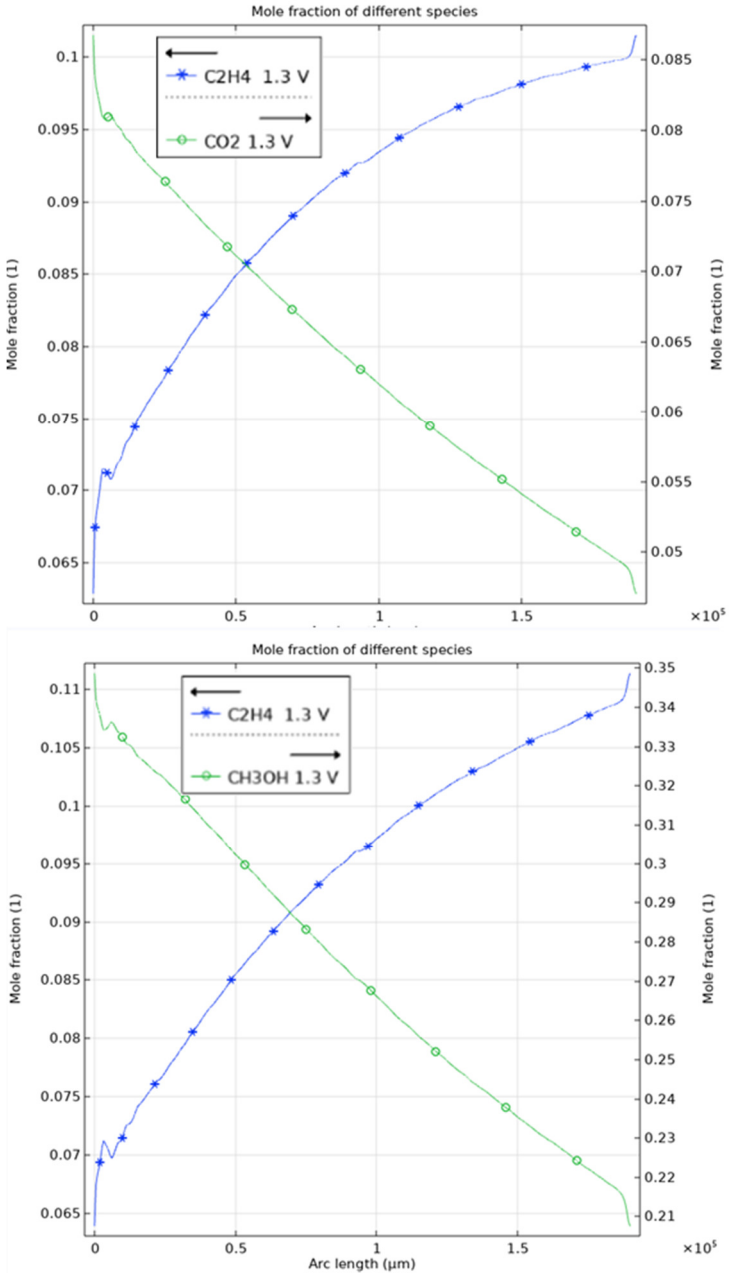


***Figure 10.*** *Mole fraction trend along the axial direction, ethene/CO2 (above) and ethene/methanol (below) at 500°C*

### 3.6 Hydrogen Concentration and Reaction Rates

The study also examines the concentration of hydrogen at 550°C and 450°C, noting that higher hydrogen concentrations at elevated temperatures are due to increased proton conductivity in the electrolyte. Although it may appear that no hydrogen is produced electrochemically, it is actually consumed in various synthesis reactions. The overall reaction rates for FTO and MTO are higher than those for hydrogen production, a trend

*This research has received funding from the European Union under grant agreement No 101099717 – ECOLEFINS project and UK Research and Innovation (UKRI) under the UK governments Horizon Europe funding Guarantee (10079292). Views and opinions expressed are however those of the author(s) only and do not necessarily reflect those of the European Union or European Innovation Council and SMEs Executive Agency (EISMEA) or UK Research and Innovation granting authorities. Neither the European Union nor the granting authorities can be held responsible for them.*

that could be reversed at higher operating temperatures, thereby increasing hydrogen production while decreasing olefin production.

### 3.7 Interdependencies Between Ethylene and Other Species

The document further explores the interdependencies between ethylene and other species, such as ethane, $CO_2$, and methanol ($CH_3OH$). It highlights that part of the ethylene produced is consumed in the synthesis of ethane, particularly at lower temperatures, due to the exothermic nature of the hydrogenation reaction. The production of ethylene is less affected by temperature changes compared to heavier olefins because some of its formation reactions are endothermic.

### 3.8 Temperature Distribution and Thermal Management

The analysis of temperature distribution within the cell reveals significant thermal gradients, reaching critical levels above 1120 K (approximately 850°C), which pose risks to the cell's structural integrity due to thermomechanical stresses. The temperature distribution is more heterogeneous within the cathode, with lower values in the flow channel and bordering side of the gas diffusion layer (GDL) compared to outer layers. This heterogeneity is attributed to differences in the structure of the anode and cathode channels, with the anode's metallic porous material allowing slower fluid movement and reduced heat extraction through convection.

*This research has received funding from the European Union under grant agreement No 101099717 – ECOLEFINS project and UK Research and Innovation (UKRI) under the UK governments Horizon Europe funding Guarantee (10079292). Views and opinions expressed are however those of the author(s) only and do not necessarily reflect those of the European Union or European Innovation Council and SMEs Executive Agency (EISMEA) or UK Research and Innovation granting authorities. Neither the European Union nor the granting authorities can be held responsible for them.*

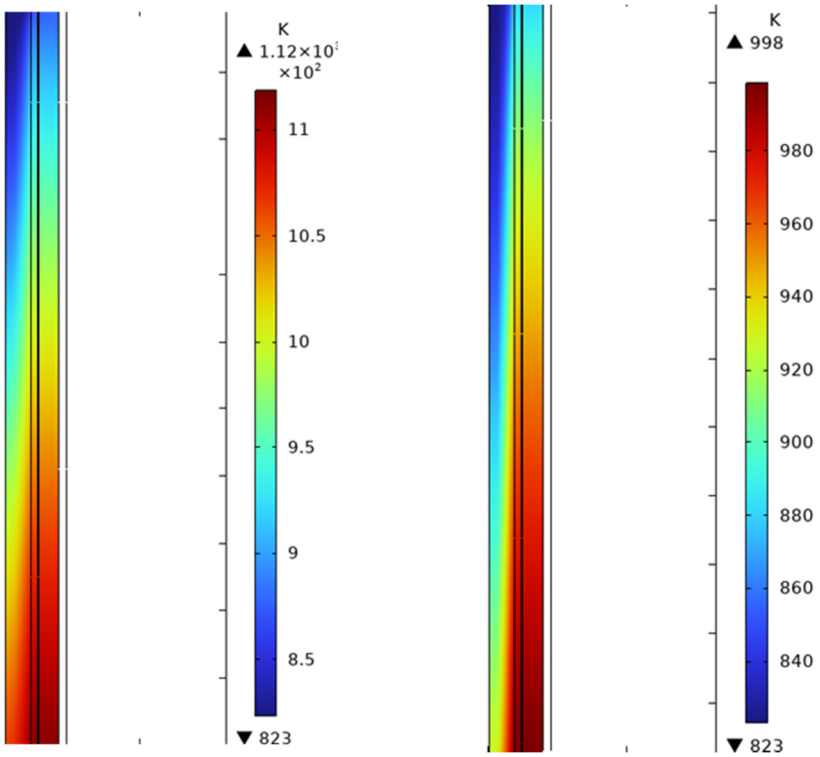


***Figure 11.*** *Temperature distribution in the cathode region with $\lambda_c$ equal to 1.5 (left picture) and 4 (right picture).*

To mitigate these thermal issues, the study proposes increasing the cathodic flow velocity to enhance heat extraction. Simulations show that increasing the flow velocity by a factor of 2.67 reduces the maximum temperature to 998 K, although significant thermal gradients persist. Further reductions in temperature could be achieved by increasing the anodic flow velocity, though this has a limited impact. An alternative approach involves performing the olefin synthesis reactions in an external reactor downstream of the cell, which could improve system reliability but increase plant complexity.

UK Research and Innovation
Funded by the European Union

*This research has received funding from the European Union under grant agreement No 101099717 – ECOLEFINS project and UK Research and Innovation (UKRI) under the UK governments Horizon Europe funding Guarantee (10079292). Views and opinions expressed are however those of the author(s) only and do not necessarily reflect those of the European Union or European Innovation Council and SMEs Executive Agency (EISMEA) or UK Research and Innovation granting authorities. Neither the European Union nor the granting authorities can be held responsible for them.*

## Conclusion

The ECOLEFINS project represents a significant advancement in the development of co-ionic ceramic reactors for sustainable olefin production. The multi-physics modelling approach has provided valuable insights into the behaviour of these reactors under various operating conditions, highlighting the importance of optimizing temperature, humidification, and flow rates to maximize performance.

The results indicate that the cross-flow configuration offers better performance in terms of ionic flux distribution and temperature management, which are critical for efficient olefin synthesis. The study also underscores the need for further calibration of model parameters and the potential benefits of performing olefin synthesis reactions in an external reactor to mitigate thermal stresses within the cell.

Future work will focus on refining the transient modelling of electrodes, calibrating model parameters with experimental data, and exploring the economic valorization of by-products such as oxygen. These efforts will contribute to the development of more efficient and sustainable technologies for olefin production, aligning with the broader goals of reducing carbon emissions and promoting a circular economy.

Funded by the European Union

*This research has received funding from the European Union under grant agreement No 101099717 – ECOLEFINS project and UK Research and Innovation (UKRI) under the UK governments Horizon Europe funding Guarantee (10079292). Views and opinions expressed are however those of the author(s) only and do not necessarily reflect those of the European Union or European Innovation Council and SMEs Executive Agency (EISMEA) or UK Research and Innovation granting authorities. Neither the European Union nor the granting authorities can be held responsible for them.*

## Bibliography

[1] H. Zhu, S. Ricote, W.G. Coors, R.J. Kee, Interpreting equilibrium-conductivity and conductivity-relaxation measurements to establish thermodynamic and transport properties for multiple charged defect conducting ceramics, Faraday Discuss. 182 (2015) 49–74. https://doi.org/10.1039/C5FD00012B.

[2] H. Zhu, S. Ricote, C. Duan, R.P. O'Hayre, D.S. Tsvetkov, R.J. Kee, Defect Incorporation and Transport within Dense BaZr0.8Y0.2O3 − δ (BZY20) Proton-Conducting Membranes, J Electrochem Soc 165 (2018) F581. https://doi.org/10.1149/2.0161809jes.

[3] R.B. Rostami, A.S. Lemraski, M. Ghavipour, R.M. Behbahani, B.H. Shahraki, T. Hamule, Kinetic modelling of methanol conversion to light olefins process over silicoaluminophosphate (SAPO-34) catalyst, Chemical Engineering Research and Design 106 (2016) 347–355. https://doi.org/https://doi.org/10.1016/j.cherd.2015.10.019.

[4] S. Najari, G. Gróf, S. Saeidi, F. Gallucci, Modeling and optimization of hydrogenation of CO2: Estimation of kinetic parameters via Artificial Bee Colony (ABC) and Differential Evolution (DE) algorithms, Int J Hydrogen Energy 44 (2019) 4630–4649. https://doi.org/https://doi.org/10.1016/j.ijhydene.2019.01.020.

[5] G. Leonzio, E. Zondervan, P.U. Foscolo, Methanol production by CO2 hydrogenation: Analysis and simulation of reactor performance, Int J Hydrogen Energy 44 (2019) 7915–7933. https://doi.org/https://doi.org/10.1016/j.ijhydene.2019.02.056.